Volume 16, Issue 3, 162415 (1-13)

Iranian Journal of Earth Science (IJES)

https://dx.doi.org/10.57647/j.ijes.2024.1603.15

3D geomechanical modelling of reservoirs in part of offshore Rio Del Rey Basin, Cameroon

Humphrey Bonjam Kunghe[1,*], Michael Adeyinka Oladunjoye[1], Kennedy Folepai Fozao[2], Lionel Takem Nkwanyang[3], Olugbenga Ademola Boboye[1]

[1]*Department of Geology, Pan African University Life and Earth Sciences Institute (PAULESI), University of Ibadan, Ibadan, Nigeria.*
[2]*Department of Petroleum Engineering, University of Bamenda, Bamenda, Cameroon.*
[3]*Department of Geology, Mining and Environmental Science, University of Bamenda, Bamenda, Cameroon.*

[*]**Corresponding author:** kunghehumphrey@yahoo.com

Original Research Paper

Received:
25 June 2023
Revised:
7 August 2023
Accepted:
15 October 2023
Published online:
15 July 2024

Abstract:

The lack of good knowledge about geomechanical parameters can be a big challenge in drilling new oil and gas wells or stimulating existing ones since geomechanical parameters are needed for safe and stable drilling. In this work, elastic parameters were determined from well logs using empirical correlations. The software used were Schlumberger Petrel 2017 and Microsoft Excel 2016. The elastic parameters determined include seismic velocity ratio (*Vp*/*Vs*), shear modulus, bulk modulus, Poison's ratio, Young's modulus, acoustic impedance, shear impedance, Lamda-Rho and Mu-Rho. The results of the elastic properties obtained from well logs were then integrated into a 3D geomechanical model to generate the spatial and depth distribution of the properties in the study area. The obtained results showed that the velocity ratio varies between 1.00 to 3.25, shear modulus varies between 1.00 GPa to 3.35 GPa, bulk modulus varies between 7.5 GPa to 13.0 GPa, Poisson's ratio varies between 0.20 to 0.48 and Young's modulus varies between 0.50 GPa to 5.0 GPa. The spatial distribution of the properties revealed potential areas for drilling new wells, targeting the southern and the eastern portions of the area that are still undrilled. The results of this study coupled with the required rock physics and geomechanical information are of great importance for drilling or hydraulic fracturing of wells in this portion of the Rio Del Ray Basin.

Keywords: Rio Del Rey Basin; Geomechanical model; Elastic properties; Drilling; Well logging

1. Introduction

The knowledge of geomechanics is very important in all stages of oil and gas exploration and production, especially elastic parameters that have proven over time to give clear information about the lithology, fluid saturation and mechanical behaviour of sedimentary rocks (Zoback, 1992). Examples of some of the elastic parameters that play a vital role include; Seismic velocity ratio (*Vp*/*Vs*), where *Vp* is the velocity of the compressional or P wave, and *Vs* is the velocity of the shear or S wave; Shear modulus (*G*), bulk modulus (*K*), Poison's ratio (ν), Young's modulus (*E*), acoustic impedance (*Ip*) and shear impedance (*Is*). These parameters when spatially distributed in a 3D model give a better picture of the hydrocarbon-bearing formations. The Sonic log measures the intervals transit time (Δtp and Δts) required for compressional and shear waves to traverse within one foot of formation. These intervals transit time are the reciprocal of compressional and shear wave velocity (Castagna et al., 1985; Johnston and Christensen, 1993). Zong et al. (2017) proposed a novel AVO inversion approach with Bayesian inference for broadband seismic data. The approach estimates low-frequency components of elastic parameters in the complex frequency domain, setting a foundation for the final estimation of absolute elastic pa-

rameters. Synthetic and field data examples demonstrate its effectiveness.

Chen and Zong (2022) developed a model using acousto-elasticity theory to formulate P- and S-wave moduli and density in biaxial-stress-induced anisotropic media. They proposed stress-dependent anisotropy parameters, introduced stress-induced anisotropy factors (SIAF), and established an approximate formula for the PP-wave reflection coefficient (that is, the ratio of the amplitude of reflected P-wave to the amplitude of incident P-wave) using scattering theory. Numerical results demonstrated the impact of horizontal biaxial stress on reflection coefficients, and inversion examples illustrated the feasibility of estimating SIAF using their proposed method. These findings contribute to the understanding of biaxial stress effects on anisotropy and wave propagation in stress-induced anisotropic media.

Many researchers have estimated the elastic properties of rocks from well logs (Eyinla and Oladunjoye, 2014; Abijah and Akaha, 2016; Alexeyev et al., 2017; Harry et al., 2018). Some recent works have used both well log data, seismic data and some supporting information such as checkshot to determine and spatially distribute elastic parameters in a 3D model (Finisha et al., 2018; Osaki et al., 2018; Agoha et al., 2021; Marbun and Haris, 2021; Dehghan and Yazdi, 2023). The present work is focussing on a study area located offshore of Rio Del Rey Basin, South West region of Cameroon. This part of the Rio Del Rey Basin is still having very limited knowledge about the geomechanical behaviour of the formation rocks. Recent works offshore of Rio Del Rey Basin have focused mostly on petrophysical analysis and the generation of prospect maps of the reservoirs. Examples of such works include the works of Fozao et al. (2018), Nkwanyang et al. (2018), and Nkwanyang et al. (2021). The objectives of the current study are to determine the elastic parameters (velocity ratio, Young's modulus, bulk modulus, shear modulus, Poisson's ratio, acoustic impedance, Lamda-Rho and Mu-Rho) using well logs and empirical correlations; And secondly, to generate a spatially distribution of these parameters in a 3D geomechanical model.

2. Geology of the study area

The Rio Del Rey (R.D.R) Basin is one of the two coastal basins in Cameroon that are actively producing. It is located in the southwestern region of Cameroon between latitude 4° and 5° North and longitude 8°20′ and 9°10′ East (Fig. 1). According to Coughlin et al. (1993), it is the eastern extension of the neighbouring Niger Delta Basin of Nigeria. The offshore area covered by the Rio Del Rey Basin is approximately 7000 km^2 and the central part of the basin has the richest hydrocarbon potentials estimated to be about six kilometres thick. The Rio Del Rey Basin shares a border with Nigeria's Niger Delta Basin to the west and northwest, to the south by Equatorial Guinea's Rio Muni Basin, to the north by the Rumpi hills, and to the east by Douala/Kribi-Campo Basin. The Rio Del Rey (R.D.R) is separated from the Douala/Kribi-Campo Basin by the Cameroon Volcanic Line (CVL), which is a line characterized by volcanic activities in Cameroon (Doust and Omatsola, 1990; Coughlin et al., 1993; Lawrence et al., 2002).

The rifting process that formed the Gulf of Guinea and separates the African and South American continents in the

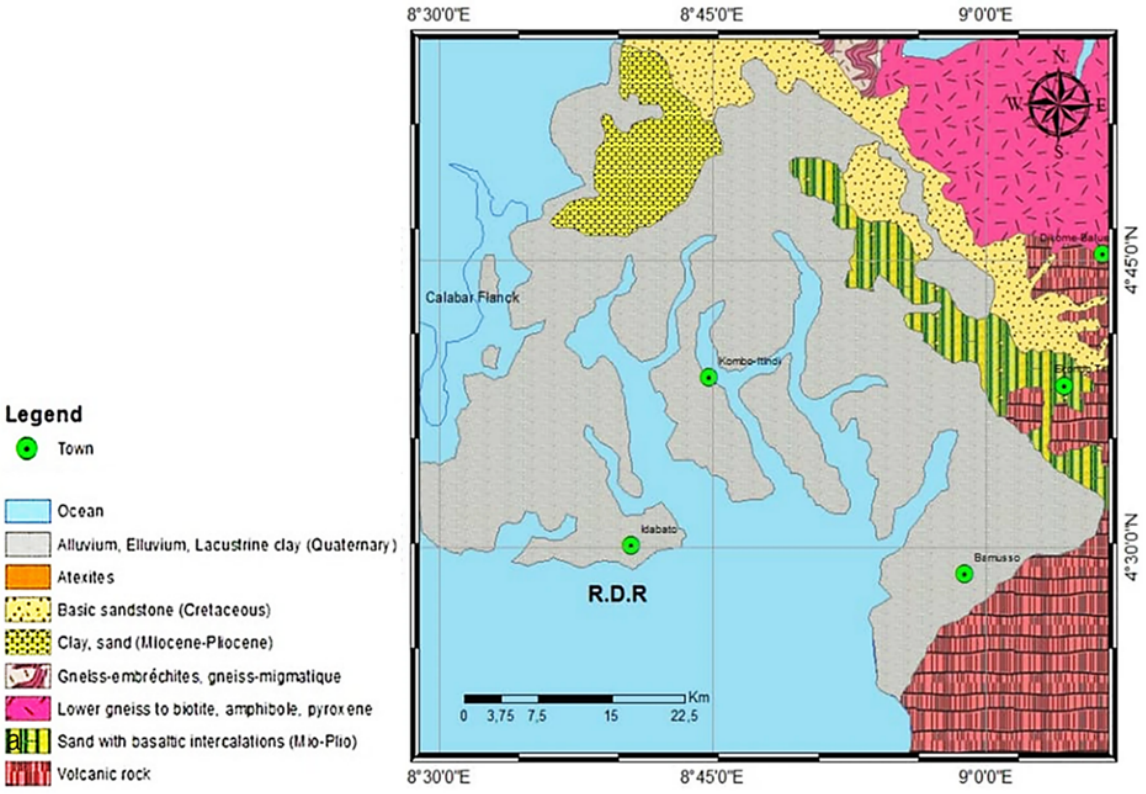

Figure 1. Geologic map of the Rio Del Rey Basin (adapted from Dumort, 1968).

Albo-Aptian period, is closely related to the development and tectonic evolution of the Rio Del Rey Basin (Lawrence et al., 2002). There are three stages that gave rise to the tectonic evolution of the Rio Del Rey Basin, which include: The Pre-rift stage which is aged from the Late Proterozoic to the Late Jurassic, it consists of continental deposits of clastic rocks from the Carboniferous to the Jurassic; The Syn-rift stage consisting of a thick sequence of fluvial and lacustrine deposits ranging from the Late Jurassic to the Early Cretaceous; The Post-rift stage consisting of a range of ages from the late Cretaceous to the Holocene. It includes progradation units and shelf clastic and carbonate rocks, as well as open ocean water (Brownfield and Charpentier, 2006; Villemin and Tarreserence, 1990).

The Rio Del Rey Basin has a stratigraphy similar to that of the Niger Delta Basin (Fig. 2). It comprises three main diachronic formations, which include: The Akata Formation having the age Late Paleocene, and was deposited in the prodeltaic marine environment consisting mostly of clays; The Agbada Formation with the age of Oligocene to Miocene, which was deposited in the delta front environment above the Akata Formation and consisting of intercalation of sand and clay; The Benin Formation consisting of continental sands and sandstones with rare shale, which was deposited in the environment of the coastal plain.

3. Methodology

The study was carried out using well log data of ten wells pseudo-named wells A, B, C, D, E, F, G, H, I and J for confidentiality of the data. The well logs comprise of gamma ray, resistivity log, sonic log, density log and caliper log. Additional data used include: 2D seismic data and checkshot for all the study wells. Schlumberger Petrel 2017 and Microsoft Excel 2016 were the two main tools used to carry out the work. Firstly, the compressional and shear wave velocities were generated from sonic logs These velocities together with empirical correlations were then used to determine all the elastic properties including velocity ratio (*Vp*/*Vs*), Young's modulus, bulk modulus, shear modulus, Poison's ratio, acoustic impedance, Lamda-Rho and Mu-Rho. Well to seismic tie was carried out by generating synthetic seismogram from well logs (density and sonic logs) and then comparing to the seismic section. A 3D model, which consisted of a framework of skeleton and the structure of the

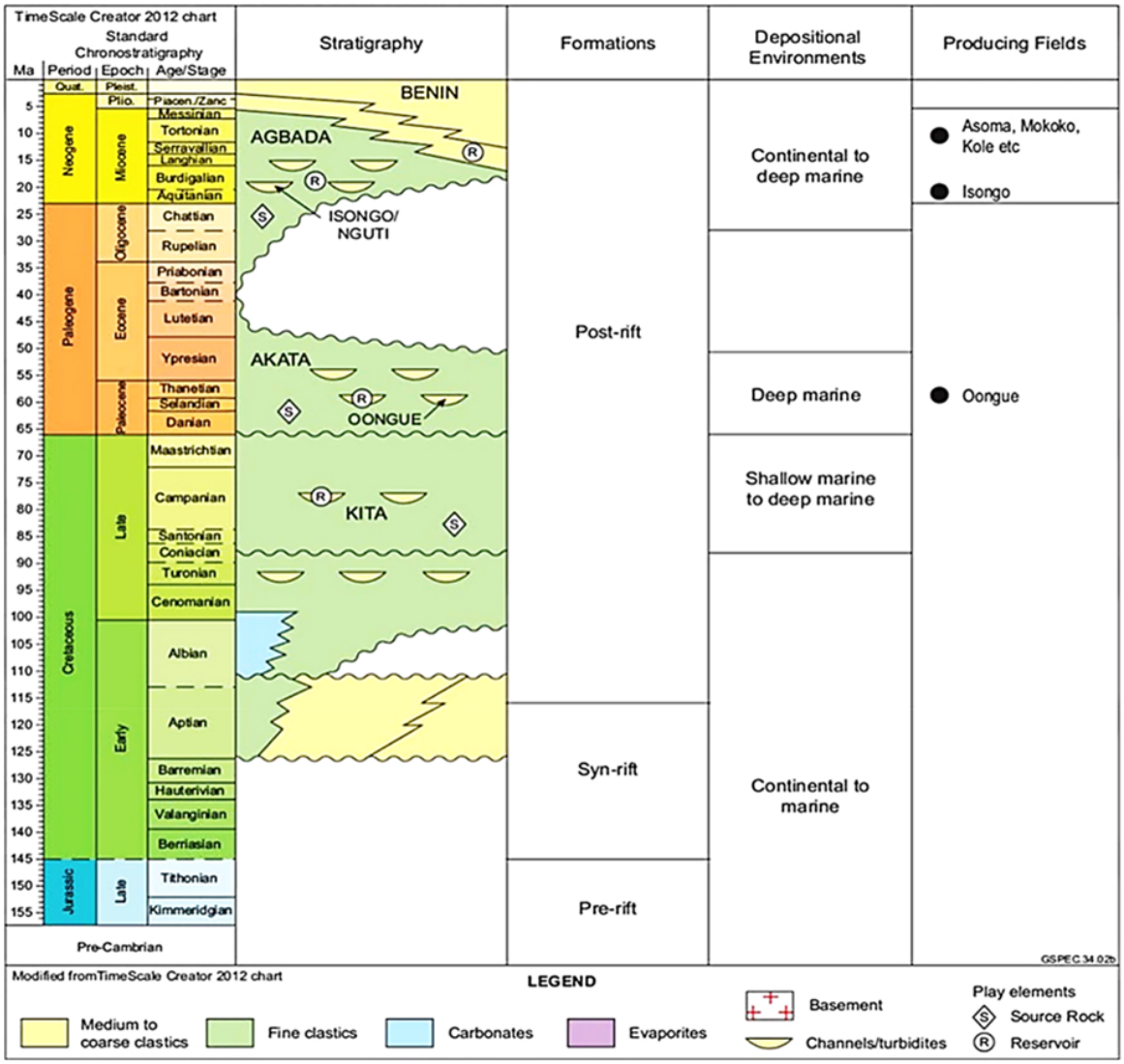

Figure 2. Stratigraphy of the Rio Del Rey Basin showing the three main formations (adapted from SNH, 2019).

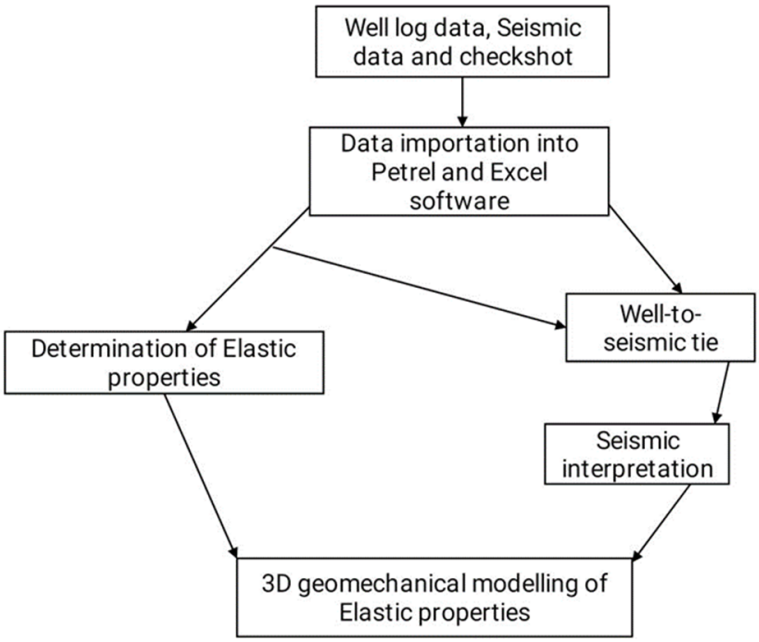

Figure 3. Workflow used to carry out 3D geomechanical modelling of elastic properties in offshore, Rio Del Rey.

model, was generated. The elastic parameters were then up-scaled and distributed into the geologic model. Figure 3 shows the workflow that summarizes the main steps used to carry out the research.

3.1 Shear wave velocity determination

In the study wells, compressional wave velocity was available but shear wave velocity was missing since it is not commonly logged. The shear wave velocity (Vs) was determined from the empirical relation between compressional wave velocity and shear wave velocity, which is commonly applied in clastic sedimentary rocks (Greenberg and Castagna, 1992) (Eq. 1). This is justified by the fact that the sedimentary rocks of the Rio Del Rey Basin are clastic in nature.

$$Vs = 0.804 \times Vp - 0.85 \quad (1)$$

where Vp is the compression wave velocity and Vs is the shear wave velocity, in (m/s).

3.2 Shear Modulus (G) determination

Shear modulus (G) is the ratio of the stress applied on a material to the change in shape or distortion. It is the ratio of the shear stress to the shear strain in a material. Shear modulus relies fully on bulk density and on shear wave velocity. The SI (International System of Units) unit of shear modulus is Pascal. It is expressed mathematically as follows (Schlumberger, 1989) (Eq. 2).

$$G = \rho\, Vs^2 \quad (2)$$

where G = shear modulus in Pa, ρ = density in kg/m^3.

3.3 Poisson's Ratio (ν) determination

Poison's ratio (ν) is the measure of the ratio of the lateral strain of a material to the longitudinal strain of the material. In other words, it is a measure of how much the diameter or width of a given material will change when it is pulled longitudinally or lengthwise (Chang et al., 2006). Many materials have Poisson's ratio values between 0 and 0.5, although some materials have negative Poisson's ratio (Gercek, 2007). The Poisson's ratio can reach 0.5 for very flexible materials like rubber, while Poisson's ratio for very stiff materials such as concrete is 0.1. Because Poisson's ratio contributes to the deformation of elastic materials, it plays a crucial role in rock engineering problems, such as numerical stress analysis. Table 1 shows some ranges of Poisson's ratio in different rocks (Chang et al., 2006; Wendt et al., 2007; Zoback, 2007).

Poisson ratio (ν) was determined in this work from compressional and shear wave velocities using Eq. 3.

$$\nu = \frac{Vp^2 - 2\,Vs^2}{2(Vp^2 - Vs^2)} \quad (3)$$

where ν = Poisson's ratio (dimensionless).

3.4 Young's Modulus (E) determination

According to Fjær et al. (1992), Young's modulus (E) is the ratio of the extensional stress to the extensional strain,

Table 1. Common values for Poisson's ratio (Gercek, 2007).

Lithology	Dolomite	Limestone	Sandstone	Shale	Siltstone
Poisson's ratio	0.1–0.35	0.1–0.325	0.05–0.4	0.05–0.325	0.12–0.35

which is the ability of the rock to resist compressional forces from uniaxial stresses. In other words, it is the ratio of the linear effort applied to an object to the change in dimension of the original length of the material. Young modulus is a mechanical property that relies on Poisson's ratio and shear modulus. Young's modulus is also known as the modulus of elasticity. It was estimated using Eq. 4 (Chang et al., 2006).

$$E = \frac{\rho\, Vs^2(3\,Vp^2 - 4\,Vs^2)}{Vp^2 - Vs^2} \tag{4}$$

where E = Young's modulus in Pa.

3.5 Bulk Modulus (K) determination

Bulk modulus (K) is an elastic property that measures how the material will compress when a given amount of external pressure or stress is applied to it. In other words, it is the ratio of applied stress to the change in the volume of material (Gatens et al., 1990). Bulk modulus depends on the bulk density, compressional wave and shear wave interval transit time. It is also known as compressibility modulus. It defines the numerical constant of the elastic properties of a solid or fluid when pressure is applied (Economides and Nolte, 2000). It was calculated using Eq. 5. The applied pressure decreases the volume of a rock, which comes to its original state after removing stress (Chang et al., 2006).

$$K = \rho(3\,Vp^2 - 4\,Vs^2)/2 \tag{5}$$

where K = bulk modulus in Pa.

3.6 Impedance (Ip and Is) calculation

Impedance is the product of density and velocity. Velocity can be either compression wave velocity (Vp) or shear wave velocity (Vs). The acoustic and shear impedance (Ip and Is) were derived using Eqs. 6 and 7 formulated by Goodway (2001).

$$Ip = Vp \times \rho \tag{6}$$

$$Is = Vs \times \rho \tag{7}$$

where Ip is acoustic impedance and Is represents the shear impedance.

3.7 Lame's parameters (Lamda and Mu) calculation

Lame's parameters are two material-dependent components that arise in the strain-stress relationship. Lamda (λ) defines incompressible rocks, whereas Mu (μ) defines rigid rocks. Lamda and Mu can be derived from Eqs. 8 and 9 (Goodway et al., 1996; Goodway, 2001; Ji et al., 2010). Lamda-Rho ($\lambda\rho$) and Mu-Rho ($\mu\rho$) parameters were calculated using Eqs. 10 and 11 proposed by Goodway et al. (1996).

$$\lambda = Vp^2 \times \rho - 2\,Vs^2 \times \rho \tag{8}$$

$$\mu = Vs^2 \times \rho \tag{9}$$

$$\lambda\rho = Ip^2 - 2\,Is^2 \tag{10}$$

$$\mu\rho = Is^2 \tag{11}$$

where λ is incompressibility in Pa, $\mu = G$ is the rigidity in Pa, Ip is acoustic impedance in Pa $\cdot$ s/m and Is represents shear impedance in Pa $\cdot$ s/m.

3.8 3D Geomechanical modelling

The 3D geomechanical models of the elastic properties including velocity ratio, shear modulus, bulk modulus, Poisson's ratio, and Young's modulus were built. A stochastic method was selected to interpolate the elastic parameters to contain the continuous data density in the study. The spatial distribution of the elastic parameters was generated by pillar gridding, upscaling of well logs and using the sequential Gaussian simulation with a collocated co-kriging algorithm. Variogram modelling was also used to check and control the spatial distribution of the elastic properties in the areas out of the location of the wells.

4. Results

The average values of the estimated elastic parameters including S-wave velocity, shear modulus, bulk modulus, Poisson's ratio, Young's modulus, velocity ratio, acoustic impedance, shear impedance, Mu-Rho and Lamda-Rho in well-B are 513 m/s, 1.70 GPa, 7.55 GPa, 0.42, 5.70 GPa, 2.53, 4002 kPa $\cdot$ s/m, 2107.3 kPa $\cdot$ s/m, 5.60E+12 kg^2/s^2 $\cdot$ m^4 and 2.30E+13 kg^2/s^2 $\cdot$ m^4 respectively. The average values of S-wave velocity, shear modulus, bulk modulus, Poisson's ratio, Young's modulus, velocity ratio, acoustic impedance, shear impedance, Mu-Rho and Lamda-Rho in well-D are 475.2 m/s, 6.07 GPa, 12.05 GPa, 0.38, 7.26 GPa, 2.66, 6905 kPa $\cdot$ s/m, 2430.1 kPa $\cdot$ s/m, 5.31E+12 kg^2/s^2 $\cdot$ m^4 and 2.15E+13 kg^2/s^2 $\cdot$ m^4 respectively. The average values of S-wave velocity, shear modulus, bulk modulus, Poisson's ratio, Young's modulus, velocity ratio, acoustic impedance, shear impedance, Mu-Rho and Lamda-Rho in well-I are 750.8 m/s, 2.37 GPa, 6.43 GPa, 0.41, 6.72 GPa, 3.25, 4450 kPa $\cdot$ s/m, 2701 kPa $\cdot$ s/m, 6.90E+12 kg^2/s^2 $\cdot$ m^4 and 3.25E+13 kg^2/s^2 $\cdot$ m^4 respectively. The average values of the estimated elastic parameters in the other study wells are similar to the values presented above.

Figures 4 to 6 represent the depth profile plots of S-wave velocity, shear modulus, bulk modulus, Poisson's ratio, Young's modulus, velocity ratio, acoustic impedance, shear impedance, Mu-Rho and Lamda-Rho displayed for example in wells B, D and I. In each of the wells, track 1 is depth, track 2 is gamma log, track 3 is the sonic log, track 4 represents density and neutron, track 5 is facies, track 6 is S-wave velocity, track 7 represents acoustic and shear impedance, track 8 is velocity ratio, track 9 is Poisson's ratio, track 10 represents shear modulus, Bulk modulus and Young's modulus and lastly track 11 represents Mu-Rho and Lamda-Rho.

Fig. 7 shows the outcome of the seismic to well tie that integrated the well and seismic data in this work to effect the geomechanical model. Figs. 8(a) to 8(e) represent the results of the 3D models showing penetrated wells and the spatial distribution of different elastic parameters. The elastic parameters included in the model include velocity ratio model, shear modulus model, bulk modulus model, Poisson's ratio and Young's modulus model. The arrow in each of the models is pointing to the north (N) direction.

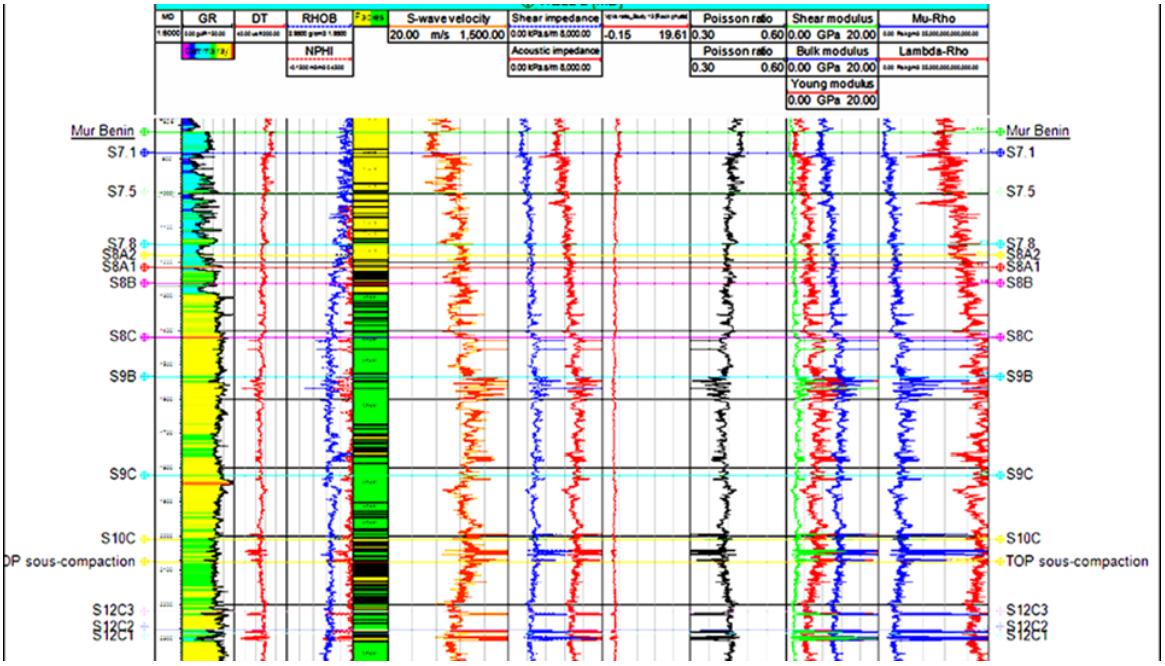

Figure 4. Log profiles of the elastic properties in well-B.

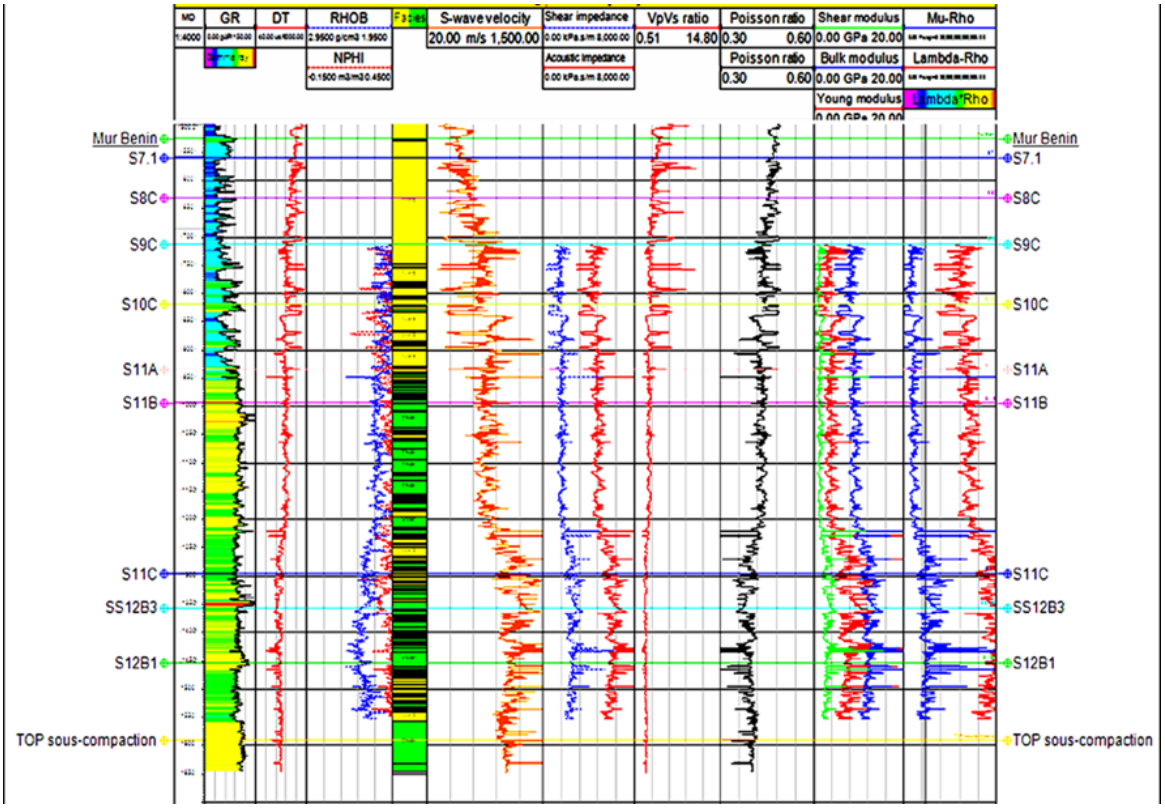

Figure 5. Log profiles of the elastic properties in well-D.

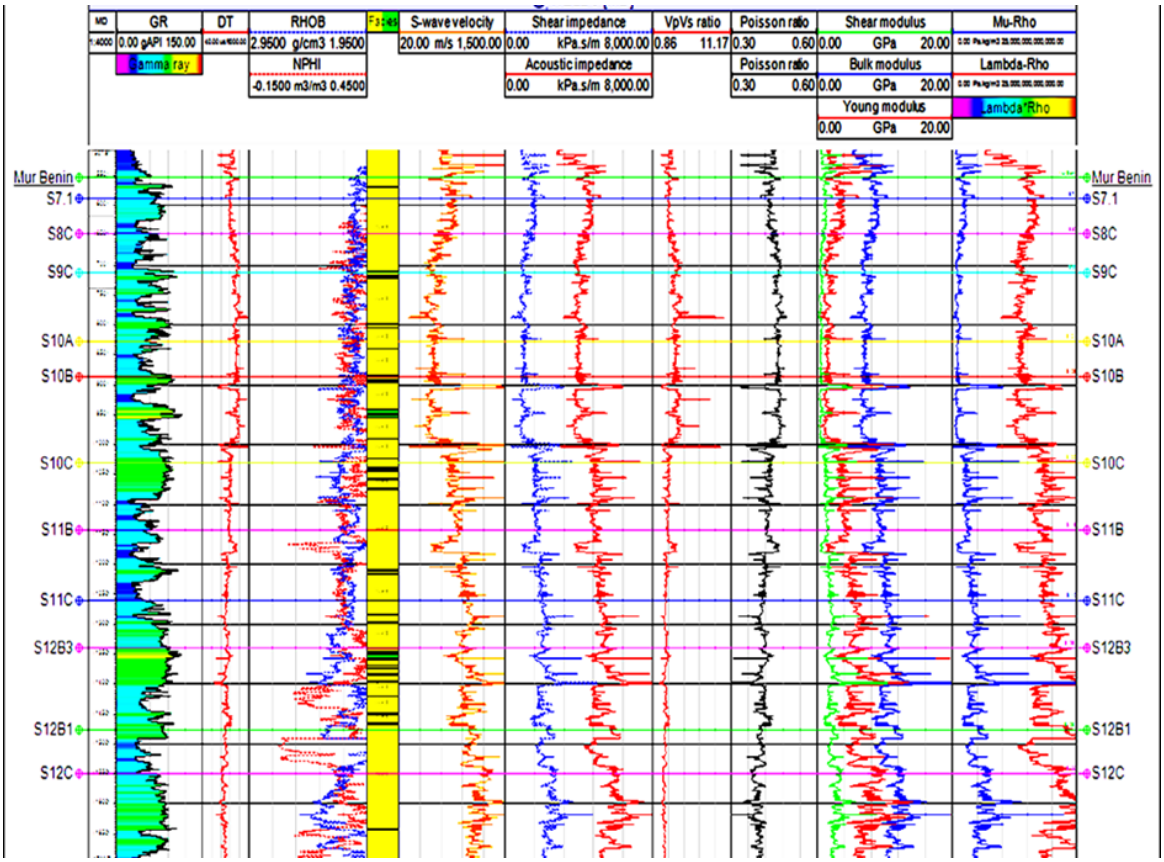

Figure 6. Log profiles of the elastic properties in well-I.

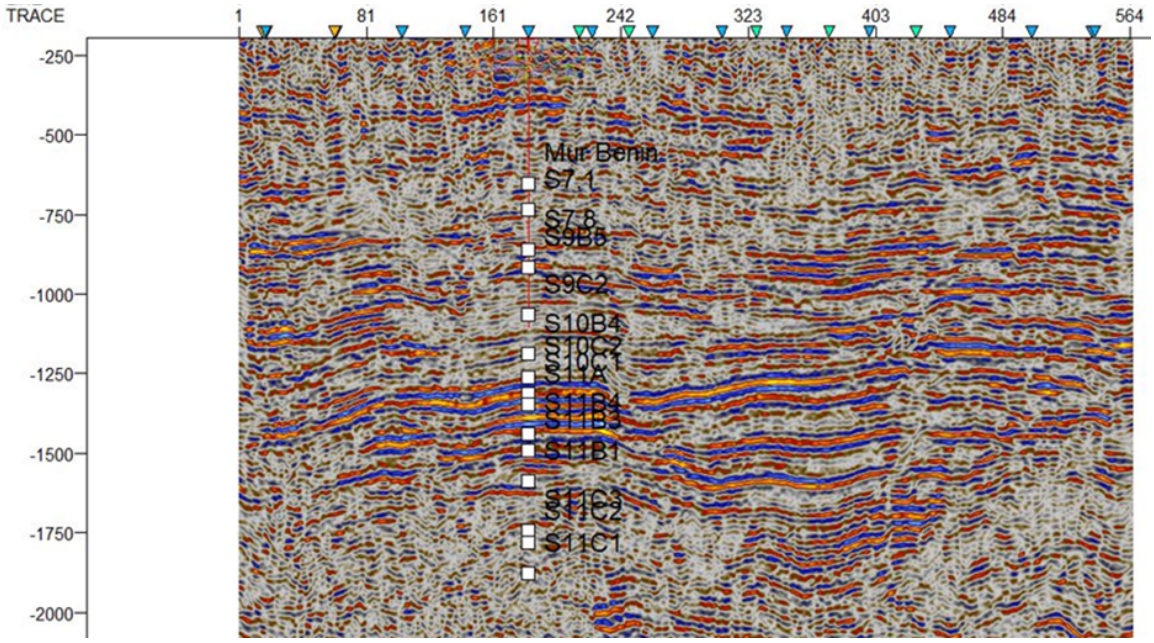

Figure 7. Integration of well-H and seismic data in the study area.

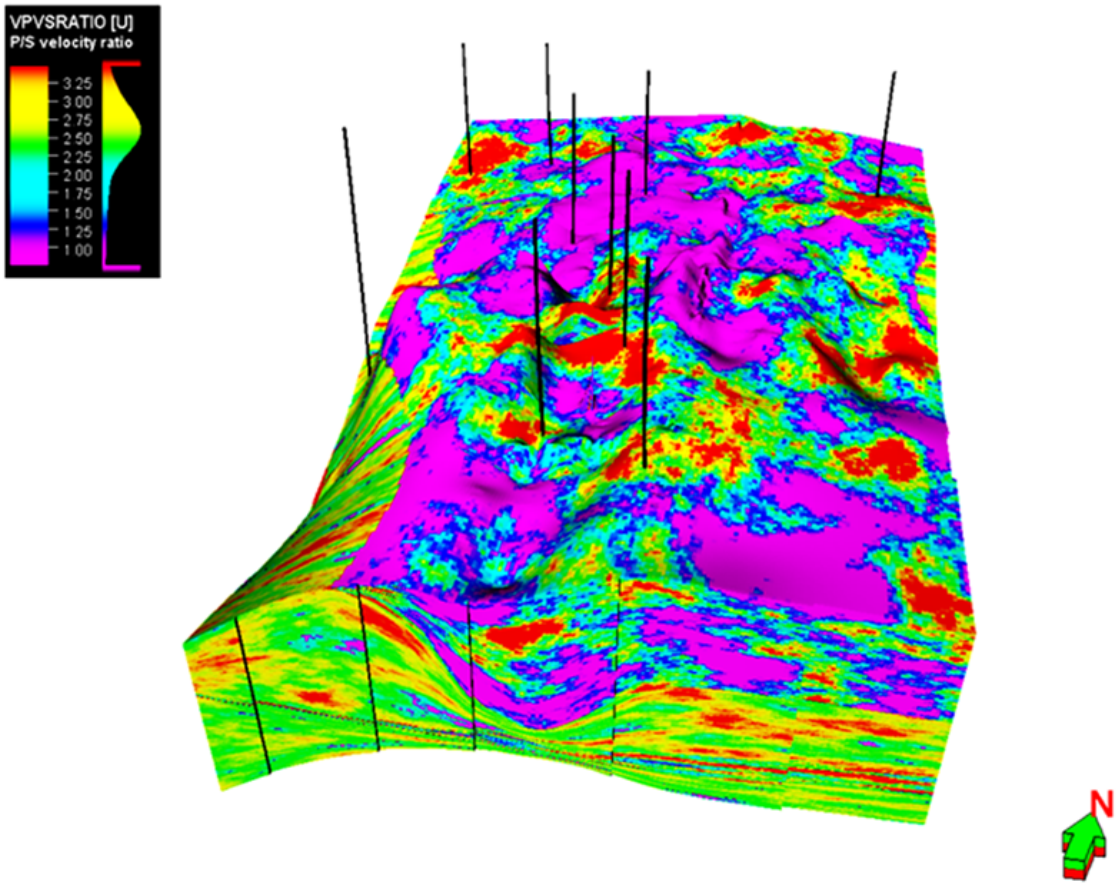

Figure 8(a). 3D Geomechanical model showing penetrated wells and spatial distribution of velocity ratio.

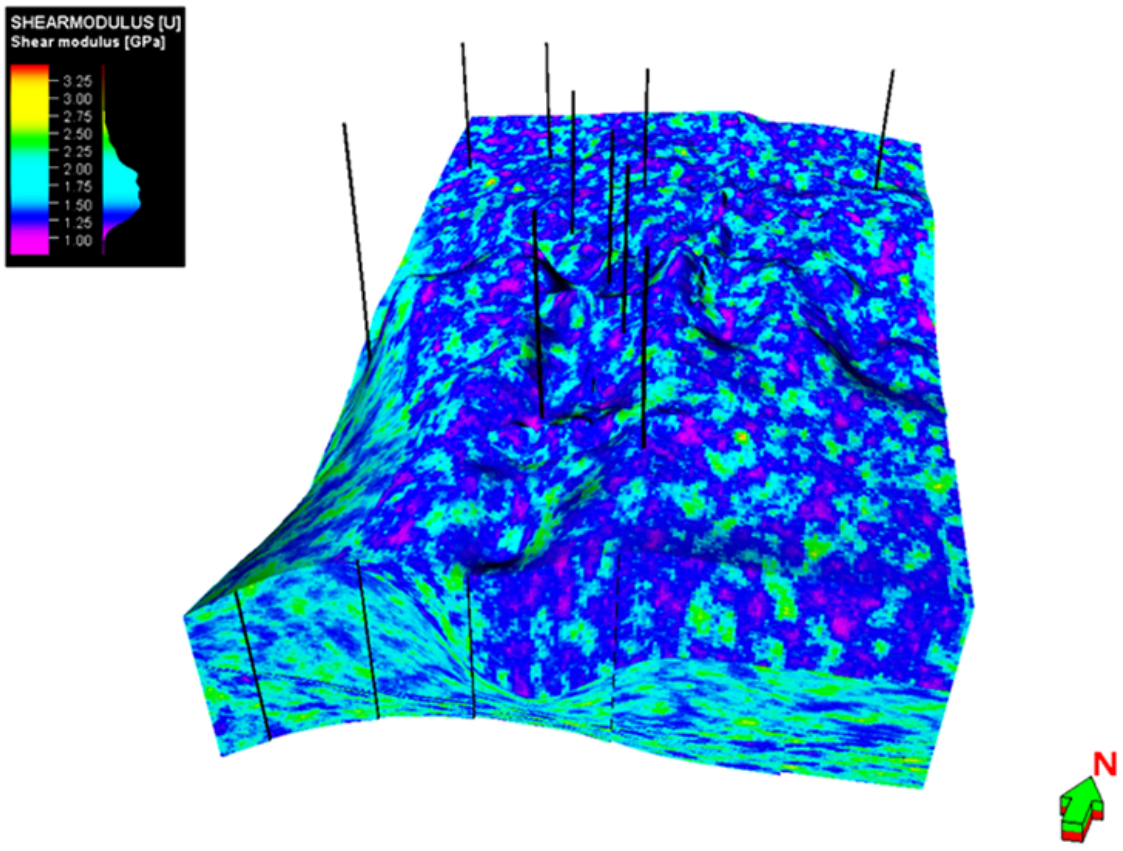

Figure 8(b). 3D Geomechanical model showing penetrated wells and spatial distribution of shear modulus.

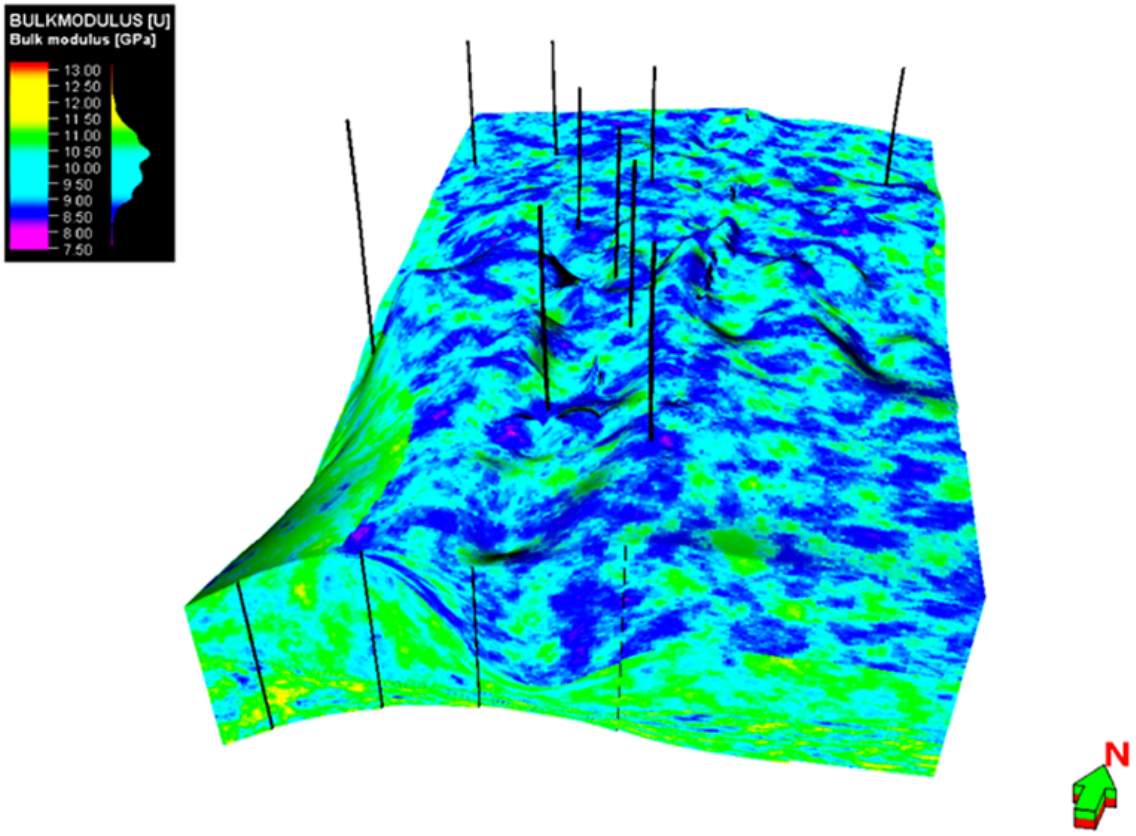

Figure 8(c). 3D Geomechanical model showing penetrated wells and spatial distribution of bulk modulus.

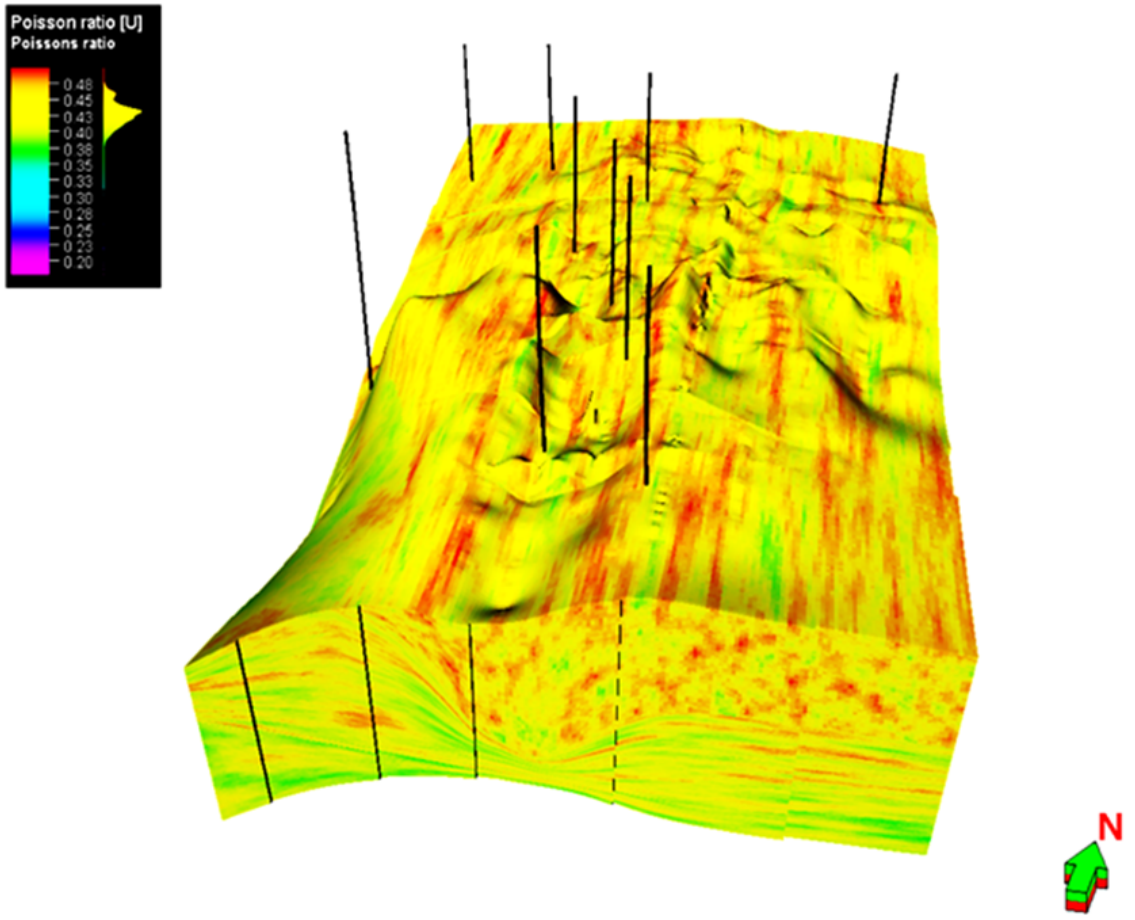

Figure 8(d). 3D Geomechanical model showing penetrated wells and spatial distribution of Poisson's ratio.

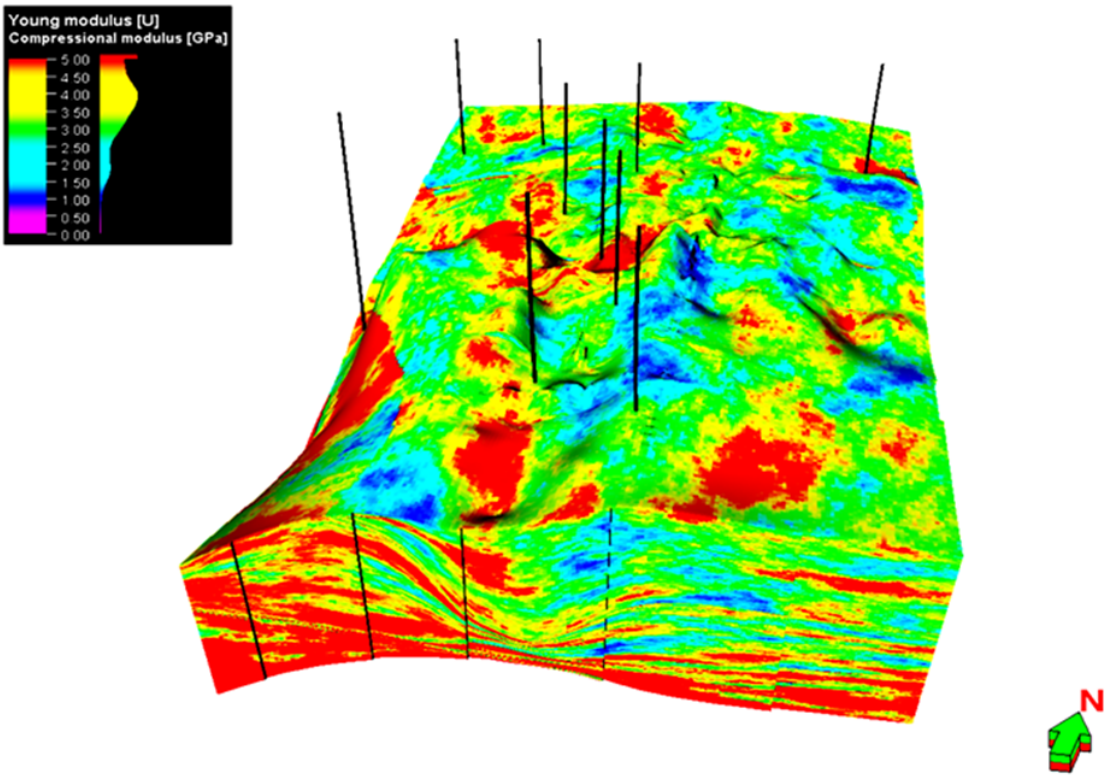

Figure 8(e). 3D Geomechanical model showing penetrated wells and spatial distribution of Young's modulus.

5. Discussion

The interpretation shows that the study data was recorded within the Agbada Formation starting from the base line of the Benin Formation "Mur Benin" and penetrated deeper into the Agbada Formation. The well log data fall at a depth interval between 500 m to 3000 m. The elastic properties generally increase with depth. This implies that the deeper shale zones will resist deformation more than the shallow sand zones that will deform fast when subjected to high conditions of stress during the drilling of new wells or stimulating existing ones (Agoha et al., 2021). Rock failure has little or no dependence on lithology but fully depends on compaction due to the weight of overburdened formations, thus increase in strength. Rock failure also depends strongly on the strength of the rocks as well as the concentration of in-situ stress (Kunghe et al., 2023). The results of the computed elastic parameters in this work are similar to the findings of Emujaporue and Ekine (2009) who determined elastic parameters in the western portion of the Niger Delta Basin. The results also show a clear similarity to the work of Eyinla and Oladunjoye (2014). The same similarity can be seen in the work of Dein et al. (2019) who determined the geomechanical properties of Niger Delta reservoir rocks using well log data.

The interpretation of the spatial distribution of elastic properties in the 3D model is according to the colour legend and potential undrilled areas in the field are easily spotted. Targeted areas are the southern and the eastern portions of the field, which are still undrilled but have good potentials of hydrocarbon (Figs. 8(a) to 8(e)). The presence of hydrocarbons in this area was confirmed by the petrophysical property model, which is part of this study but not included in this article. It is recommended to drill in areas with high elastic parameters as these areas will resist deformation during drilling (Agoha et al., 2021). From the 3D models of elastic parameters, the velocity ratio varies between 1.00 to 3.25. The velocity ratio varies slightly laterally but increases greatly with depth. The high percentage of the velocity ratio at deeper depths in the model is a result of the high percentage of shale with depth since the velocity ratio tends to show high values in shale than in sand lithology (Castagna et al., 1985).

The distribution of the shear modulus in the model shows low values in shallow zones, while the deeper zones show relatively high values. The model also shows lateral homogeneity. The model shows that the values of the shear modulus vary from 1.00 GPa to 3.00 GPa, which agrees with the results of the shear modulus obtained from well logs. This means that the field should not be subjected to stress above this variation to maintain stability during drilling (De Souza et al., 2014). The distribution of the bulk modulus is similar to that of the shear modulus, which shows relatively low values at shallow depths, whereas there is a great increase with depth. The values of the bulk modulus in the model vary from 8.00 GPa to 13.00 GPa. To maintain stability during drilling or hydraulic fracturing, this range should be maintained when drilling new wells in the area, and during hydraulic fracturing (Agoha et al., 2021).

The model shows an even distribution of Poisson's ratio laterally and vertically in the field. The even distribution of Poisson's ratio is a result of the shaly nature of the reservoirs, which causes a high Poisson's ratio and consequently high ductility of formation rocks. The values of Poisson's

ratio in the model vary from 0.35 to 0.48. The distribution of Young's modulus in the field shows a small lateral variation and significant vertical changes with depth. The increase in Young's modulus with depth is a result of an increase in compaction or compression from overburdened formations. This is because Young's modulus measures the ability of a material to withstand or resist changes in length when subjected to lengthwise tension or compression. The model shows that Young's modulus varies from 1.0 GPa to 5.0 GPa. It is however recommended to maintain this range during drilling or hydraulic fracturing (Agoha et al., 2021). The results of the 3D models, however, correspond with the findings of Finisha et al. (2018) who integrated 2D seismic data with well logs to carry out 3D geomechanical modelling for the distribution of elastic properties in an area located Onshore of Northwest Java Basin, Indonesia. The present work is also in agreement with the works of Osaki et al. (2018) who carried out 3D geomechanical modelling of the reservoirs and revealed the spatial and lateral distribution of elastic properties in an area located in the Niger Delta, Nigeria. The current work also agrees with the work of Agoha et al. (2021) who worked on integrated 3D geomechanical modelling in a field located offshore Niger Delta, Southern Nigeria.

6. Conclusion

The 3D geomechanical model successfully proposed the distribution of elastic parameters in the study area and the variation of the parameters was also included in the model. Elastic or mechanical properties of rocks greatly control the problems faced during the drilling and development of hydrocarbon fields. Such problems can be mitigated if the results of the elastic properties and their spatial distribution in the hydrocarbon field are well understood, especially through inclusive 3D geomechanical modelling. An understanding of reservoir geomechanics is imperative for the successful exploration and exploitation of hydrocarbons especially in a complex and tertiary basin like the Rio Del Ray Basin. It can be concluded that the integration of well logs and seismic data can effectively model the spatial distribution of elastic properties in the study area. The results obtained in this work can complement the required rock physics and geomechanical information needed for drilling or hydraulic fracturing.

Acknowledgment

The authors are thankful to the African Union Commission for the financial support to the first author. The authors are grateful to the Editor in Chief and the anonymous reviewers for their invaluable suggestions.

Authors Contributions

All authors have contributed equally to prepare the paper.

Availability of Data and Materials

The data that support the findings of this study are available from the corresponding author upon reasonable request.

Conflict of Interests

The authors declare that they have no known competing financial interests or personal relationships that could have appeared to influence the work reported in this paper.

References

Abijah F.A., Akaha C.T. (2016) Geomechanical Evaluation of an onshore oil field in the Niger. *Journal of Applied Geology and Geophysics (IOSR-JAGG)* 4 (1): 99–111. https://doi.org/10.9790/0990-041199111

Agoha C.C., Opara A.I., Okeke O.C., Okereke C.N., Onwubuariri C.N., Akiang F.B., Osaki L.J., Omenikolo I.A. (2021) Integrated 3D geomechanical characterization of a reservoir: case study of "Fuja" field, offshore Niger Delta, Southern Nigeria. *Journal of Petroleum Exploration and Production Technology* 11 (10): 3637–3662. https://doi.org/10.1007/s13202-021-01244-9

Alexeyev A., Ostadhassan M., Mohammed R.A., Bubach B. (2017) Well Log Based Geomechanical and Petrophysical Analysis of the Bakken Formation. *American rock mechanics association*

Brownfield M.E., Charpentier R.R. (2006) Geology and Total Petroleum Systems of the West-Central Coastal Province (7203), West Africa. Vol. 2207-B, 52. U.S. Geological Survey Bulletin

Castagna P., Batzle M.L., Eastwood R.L. (1985) Relationships between compressional-wave and shear-wave velocities in clastic silicate rocks. *Geophysics* 50 (4): 571–581. https://doi.org/10.1190/1.1441933

Chang C., Zoback Mark D., Khaksar Abbas (2006) Empirical relations between rock strength and physical properties in sedimentary rocks. *Journal of Petroleum Science and Engineering* 51 (3–4): 223–237. https://doi.org/10.1016/j.petrol.2006.01.003

Chen F., Zong Z. (2022) PP-wave reflection coefficient in stress-induced anisotropic media and AVAZ inversion. *GEOPHYSICS,* https://doi.org/10.1190/geo2021-0706.1

Coughlin R., Bement W., Malony W. (1993) A petroleum geology of the deltaic sequence, Rio Del Rey, ofshore Cameroon. In *AAPG International Conference and Exhibition, The Hague*

De Souza A.L.S., De Souza J.A.B., Meurer G.B., Naveira V.P., Chaves R.A.P., Frydman M., Pastor J. (2014) Integrated 3D Geomechanics and Reservoir Simulation; Optimize Performance, Avoid Fault Reac- tivation. 55–58. World Oil J Publish Gulf Publishing Company

Dehghan A.N., Yazdi A. (2023) A Geomechanical Investigation for Optimizing the Ultimate Slope Design of Shadan Open Pit Mine, Iran. *Indian Geotechnical Journal,* 1–15. https://doi.org/10.1007/s40098-022-00709-w

Dein D.H., Onengiyeofori D.A., Opiriyabo H.I. (2019) Determination of Geomechanical Properties of a typical Niger Delta Reservoir Rock Using well Logs. *Asian Journal of Applied Science and Technology (AJAST)* 3 (1)

Doust H., Omatsola E. (1990) Niger delta. In *Divergent/-passive margin basins: AAPG Memoir 48,* edited by Edwards J.D., Santogrossi P.A., 239–248.

Dumort P.J. (1968) Notice explicative sur la feuille de Douala-Ouest. Direction des Mines et de la Géologie du Cameroun. *Yaoundé* 1:69.

Economides M.J., Nolte K.G. (2000) Reservoir Stimulation. 3rd John Wiley & Sons Press: New York, NY, USA

Emujaporue G.O., Ekine A.S. (2009) Determination of Rocks Elastic constants from Compressional and Shear Waves Velocities for Western Niger Delta, Nigeria. *Journal of Applied Sciences and Environmental Management* 13 (3) https://doi.org/10.4314/jasem.v13i3.55364

Eyinla D.S., Oladunjoye M.A. (2014) Estimating Geo-Mechanical Strength of Reservoir Rocks from Well Logs for Safety Limits in Sand-Free Production. *Journal of Environment and Earth Science* 4

Finisha B., Haris A., Ronoatmojo I.S. (2018) Geomechanical modeling of reservoir rock using 2D seismic inversion : Its application to wellbore stability in the onshore of Northwest Java Basin , Indonesia. In *AIP Conference Proceedings,* 020258. https://doi.org/10.1063/1.5064255

Fjær Erling, Holt R.M., Horsrud P., Raaen A.M., Risnes R. (1992) Geological aspects of petroleum related rock mechanics. *Developments in Petroleum Science,* 157–200.

Fozao K.F., Fotso L., Djieto-Lordon A., Mbeleg M. (2018) Hydrocarbon inventory of the eastern part of the Rio Del Rey Basin using seismic attributes. *Journal of Petroleum Exploration and Production Technology,* https://doi.org/10.1007/s13202-017-0412-5

Gatens J.M., Harrison C.W., Lancaster D.E., Guldry F.K. (1990) In-situ stress tests and acoustic logs determine mechanical properties and stress profiles in the Devonian shales. *SPE Reprint Series* 45:150–156.

Gercek H. (2007) Poisson's ratio values for rocks. *International Journal of Rock Mechanics and Mining Sciences* 44 (1): 1–13. https://doi.org/10.1016/j.ijrmms.2006.04.011

Goodway B. (2001) A tutorial on AVO and Lamé constants for rock parameterization and fluid detection. 1–41. Pan Canadian Petroleum Limited,Calgary,Canada

Goodway B., Chen T., Downton J. (1996) Improved AVO fluid detection and lithology discrimination using Lamé petrophysical parameters from P and S inversions. In *Integra Geoservices Inc,* 183–186. https://doi.org/10.1190/1.1885795

Greenberg M.L., Castagna J.P. (1992) Shear-wave velocity Estimation in porous rocks: Theoretical Formulation, Preliminary Verification and Applications. *Geophysical Prospecting* 40 (April 1991): 195–209. https://doi.org/10.1111/j.1365-2478.1992.tb00371.x

Harry T.A., Etuk S.E., Joseph I.N., Austin O.E. (2018) Geomechanical evaluation of reservoirs in the coastal swamp , Niger delta region of Nigeria. *International Journal of Advanced Geosciences* 6 (2): 165–172. https://doi.org/10.14419/ijag.v6i2.13762

Ji S., Sun S., Wang Q., Marcotte D. (2010) Lamé parameters of common rocks in the Earth's crust and upper mantle. *Journal of Geophysical Research: Solid Earth* 115 (6) https://doi.org/10.1029/2009JB007134

Johnston J.E., Christensen N.I. (1993) Compressional to shear velocity ratios in sedimentary rocks. *International Journal of Rock Mechanics and Mining Sciences And* 30 (7): 751–754. https://doi.org/10.1016/0148-9062(93)90018-9

Kunghe H.B., Boboye O.A., Oladunjoye M.A., Fozao K.F., Nkwanyang L.T. (2023) Rock Strength and In Situ Stress Analysis for Wellbore Instability , Fault Stress Regime Prediction , 3D Structural and Geomechanical Modelling in H-field Offshore of Rio Del Rey Basin , Southwest Region , Cameroon. *Iranian Journal of Science,* https://doi.org/10.1007/s40995-023-01455-1

Lawrence S.R., Munday S., Bray R. (2002) Regional geology and geophysics of the eastern Gulf of Guinea (Niger Delta to Rio Muni). In *The Leading Edge* https://doi.org/10.1190/1.1523752

Marbun R., Haris A. (2021) 3D Geomechanics Characterization in V Field. *Journal of Physics: Conference Series,* 012086. https://doi.org/10.1088/1742-6596/2019/1/012086

Nkwanyang L.T., Ehinola O.A., Chongwain G.M., Makoube S.E. (2021) Application of Petrophysical Evaluation and Seismic Interpretation to Generate New Prospects Map of N-Field Rio Del Rey Basin , Cameroon. *Journal of Geoscience and Geomatics,* https://doi.org/10.12691/jgg-9-3-4

Nkwanyang L.T., Ehinola O.A., Takem J.E., Nguema P., Makoube S.E., Chongwain G.M. (2018) Depositional Setting and Petrophysical Evaluation of Reservoir of the K-Field in the Western Offshore Depobelt, Rio Del Rey Basin, Cameroon. *International Journal of Geosciences* 09 (09): 528–546. https://doi.org/10.4236/ijg.2018.99031

Osaki L.J., Uko E.D., Opara A.I. (2018) 3D Geomechanical reservoir model for Appraisal and Development of Emi- 3D Geomechanical reservoir model for Appraisal and Development of Emi-003 field In Niger Delta , Nigeria. *Asian Journal of Applied Science and Technology (AJAST)* 2 (4): 276–294.

Schlumberger (1989) Log interpretation principles/applications. 13–19. Schlumberger Educational Services: Houston

SNH (2019) CAMEROON 2019 Exploration Opportunities in two Producing Basins Invest in Cameroon's Hydrocarbons Sector. 1–24.

Villemin J., Tarreserence P. (1990) Sedimentary basins of Carbon Geology and Oil systems. 117–199. Am Assoc Petro Geologists Memoir, Tulsa

Wendt A.S., Kongslien M., Sinha B.K., Vissapragada B., Newton A., Skomedal E., Renlie L., Pedersen E.S. (2007) Enhanced Mechanical Earth Modelling and Wellbore Stability Calculations Using Advanced Sonic Measurements A. In *Case Study of the HP / HT Kvitebjorn Field in the Norwegian North Sea. Society of Petroleum Engineers.SPE,* vol. 109662, 1–16. https://doi.org/10.2118/109662-MS

Zoback M.D. (2007) Reservoir Geomechanics. Cambridge University Press https://doi.org/10.1017/CBO9780511586477

——— (1992) Stress field constraints on intraplate seismicity in eastern North America. *Journal of Geophysical Research* 97 (B8) https://doi.org/10.1029/92jb00221

Zong Z., Li K., Yin X., Zhu M., Du J., Chen W., Zhang W. (2017) Broadband seismic amplitude variation with offset inversion. *GEOPHYSICS* 82 (3) https://doi.org/10.1190/geo2016-0306.1